Dissolution-Aware Hybrid Reduced-Order Modeling and Bayesian Inference for Real-Time Gas-Kick Detection in Managed Pressure Drilling

Hamza Qureshi[1] **and Bilal Siddiqui**[2]
[1]University of Swabi, Anbar Road, Swabi 23561, Pakistan
[2]Bacha Khan University, Main Umarzai Road, Charsadda 24420, Pakistan

ABSTRACT

Gas kicks remain a dominant source of unplanned events in drilling operations, particularly when narrow pressure margins and complex fluid systems compress the time available for diagnosis and response. Modern managed pressure drilling improves controllability, yet it also raises the bar for accurate, real-time inference because annular hydraulics, gas compressibility, and fluid property uncertainty interact nonlinearly with sensor signals such as pit gain, standpipe pressure, and return flow. A recurring difficulty is that dissolved gas can materially alter apparent pit-volume trends and pressure transients, while multiphase migration redistributes mass and momentum along the annulus. This paper develops a dissolution-aware state-space formulation for kick detection that couples one-dimensional transient annular transport with a thermodynamic closure for gas dissolution and mud swelling, while explicitly representing parametric and structural uncertainty in property models. The technical contribution is a structure-preserving hybrid reduced-order model that remains stable under aggressive time discretization and that is differentiable end-to-end, enabling fast Bayesian inversion of influx rate, depth, and composition proxies from streaming surface measurements. The reduced model is trained on physics-consistent trajectories rather than on raw data alone, and it enforces positivity, compressibility consistency, and mass conservation through constrained operator inference. A sequential Bayesian estimator with adaptive covariance inflation is then derived for online assimilation. Numerical studies demonstrate that dissolution-induced swelling can be disentangled from free-gas expansion in regimes where naive pit-gain heuristics fail, and that posterior uncertainty can be propagated into actionable decision thresholds without sacrificing real-time performance.

KEYWORDS

1. Introduction

Gas-kick detection is often introduced as a sensor interpretation problem, but in practice it is a coupled inference-and-control problem shaped by the fluid system, the well geometry, and the operational envelope [1]. In managed pressure drilling, surface backpressure, choke actuation, and flow-out control can suppress excursions, yet the same control actions can mask or reshape the signatures used for diagnosis. The annulus becomes a distributed dynamical system in which mass, momentum, and energy evolve under transient boundary conditions, and the observable outputs are compressed summaries of that system. The central modeling question is therefore not whether multiphase flow matters, but how to represent it with sufficient fidelity to distinguish an incipient influx from routine operational transients while remaining computationally fast enough for continuous use.

A key physical mechanism that complicates diagnosis is dissolution of gas into oil-based or synthetic-based drilling

Article info:
Hamza Qureshi and Bilal Siddiqui. *Dissolution-Aware Hybrid Reduced-Order Modeling and Bayesian Inference for Real-Time Gas-Kick Detection in Managed Pressure Drilling*. Nextqueries.

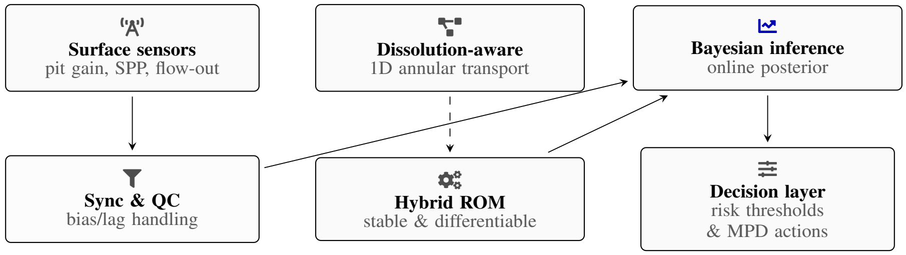

Figure 1 End-to-end real-time architecture: surface measurements are synchronized and quality-controlled, while a dissolution-aware 1D annular model supplies physics-consistent trajectories to a stable hybrid reduced-order surrogate. The differentiable surrogate enables fast Bayesian updates from streaming data and outputs uncertainty-aware risk metrics that drive managed-pressure actions (e.g., choke/backpressure adjustments) without relying on pit-gain heuristics alone.

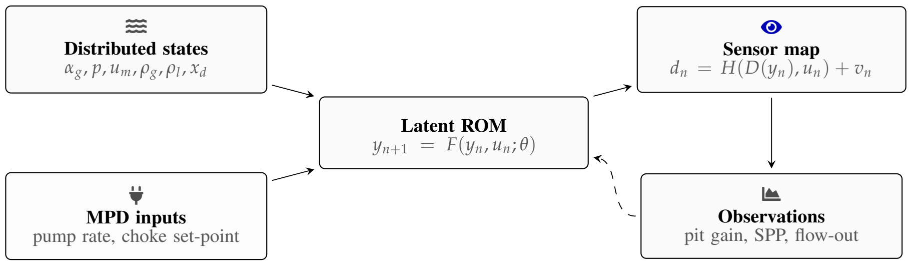

Figure 2 Dissolution-aware state-space view used for inference: distributed annular physics are compressed into a low-dimensional latent state, advanced by a reduced flow map with uncertain parameters. A sensor map predicts surface signals from decoded states, enabling sequential assimilation; a weak feedback path represents continual correction of the latent dynamics by measurement innovations.

fluids, which can yield swelling of the liquid phase and alter the pit-gain signal even when a distinct free-gas phase is not yet dominant. In this context, Manikonda et al (2020) presented a first-of-a-kind thermodynamic framework [2], based on an equation-of-state treatment of gas solubility, for estimating swelling of oil-based mud attributable to gas-kick dissolution, thereby linking dissolved-gas mole fraction to an effective formation volume factor and to pit-gain interpretation. The broader implication is that pit gain is not uniquely attributable to free-gas volume in the annulus; it is a composite of dissolution, compressibility, and transport, and any real-time inference system must include a mechanism to partition these effects.

A second practical barrier is fluid-property uncertainty, which emerges not only from measurement error but also from the limited transferability of empirical correlations across regions, compositions, and high-pressure high-temperature conditions. When property models are inaccurate, an inversion algorithm may compensate by biasing inferred influx rates or by misattributing pressure drops to frictional changes, thereby producing confident but incorrect conclusions. Sleiti et al. (2021) quantified this issue in a comprehensive assessment of gas-kick-relevant property correlations for gas-oil ratio, oil formation volume factor, gas viscosity, and gas density [3], reporting that even among better-performing models, average absolute relative errors can remain on the order of a few percent, including 3.50% to 4.45% ranges for density-based gas-viscosity formulations under high-temperature and high-pressure conditions [4]. Such errors are small enough to be ignored in steady calculations yet large enough to destabilize real-time inference when propagated through compressible multiphase dynamics and choke boundary conditions.

The dominant computational challenge is that physically detailed kick simulators can be too slow for continuous assimilation, particularly when iterative solvers, stiff closures, or fine spatial grids are required. The inference loop magnifies this cost because estimation requires repeated model evaluations, sensitivity calculations, or ensemble propagation. In the same way that high-fidelity computational fluid dynamics is rarely used inside a control loop, high-fidelity kick simulators are often relegated to offline analysis. The objective of this paper is to close that gap by constructing a reduced model that preserves the physical invariants and qualitative behavior needed for credible inference, while being sufficiently fast and differentiable to support Bayesian state estimation from streaming measurements [5].

The paper advances an integrated framework with three core elements that are designed to work together rather than as separate modules. The first element is a coupled annular transport model that represents the migrating kick as a distributed system with explicit mass exchange between dissolved and free phases, and with boundary conditions consistent with managed pressure drilling actuators. The second element is a thermodynamic swelling closure that maps pressure and temperature histories to dissolved fraction and to an effective liquid volume expansion, while remaining numerically stable in the regimes relevant to real-time simulation. The third element is a hybrid reduced-order representation built via constrained operator inference in physically meaningful coordinates, designed to preserve positivity of phase fractions and densities, and to maintain global mass conservation to machine tolerance under discrete time stepping.

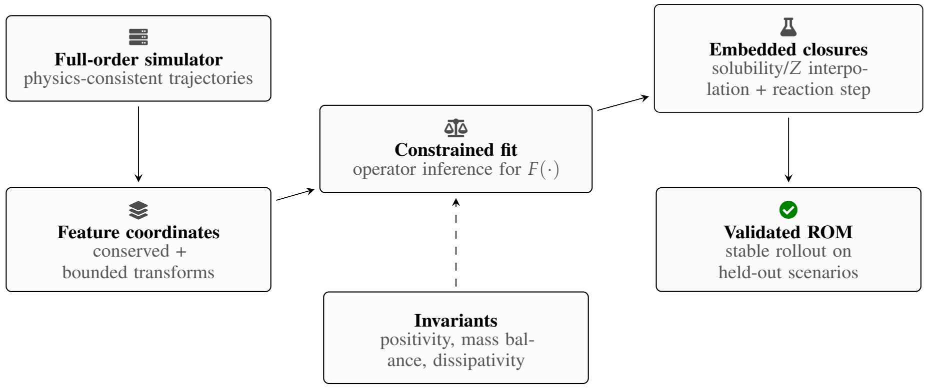

Figure 3 Structure-preserving ROM training workflow: full-order trajectories are mapped into physically meaningful coordinates (conserved variables plus bounded transforms for fractions/densities). Operator inference learns a compact time-advance map under explicit constraints, while thermodynamic lookups and a stable reaction update remain embedded rather than re-learned. Validation emphasizes multi-step rollout fidelity for sensor-relevant outputs.

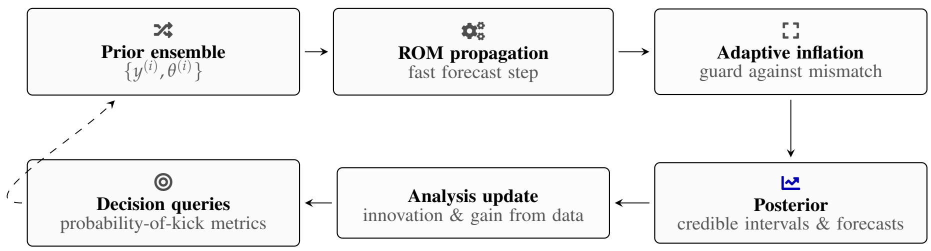

Figure 4 Sequential Bayesian assimilation on the reduced model: an ensemble of latent states and uncertain parameters is propagated cheaply, corrected using streaming observations, and stabilized with adaptive covariance inflation. The resulting posterior supports probability-based decision metrics and short-horizon what-if forecasts, enabling timely intervention under narrow pressure margins.

The novelty does not lie in asserting that these mechanisms exist, but in providing a tractable, end-to-end inference architecture that supports uncertainty quantification. The reduction is not a generic regression surrogate; it is a structured approximation of the flow operator and closure terms that respects the algebraic constraints of the physical system [6]. The inference layer is likewise not a generic filter; it is derived for the particular structure of the reduced model, including the strongly correlated uncertainties induced by property closures and sensor biases. The resulting system can produce posterior distributions over influx parameters, rather than point estimates, enabling operational thresholds to be set in terms of risk rather than in terms of deterministic residuals.

The remainder of the paper is organized as follows. The next section introduces the coupled governing equations and the sensor map used to connect downhole states to surface measurements under managed pressure drilling boundary conditions. The subsequent section develops the dissolution and swelling closure, clarifying how the thermodynamic constraints are embedded into the dynamical model without introducing stiffness that would preclude real-time use [7]. The following section presents the structure-preserving reduced-order surrogate and details the constrained operator inference procedure. The next section derives the Bayesian inversion and online assimilation method, emphasizing uncertainty propagation and identifiability. The final technical section reports numerical experiments and sensitivity analyses, and the paper concludes with implications for real-time deployment and directions for extension.

2. Coupled Annular Transport Model for Kick Migration

A drilling annulus can be modeled at multiple levels of fidelity. For real-time inference, the model must capture the primary mechanisms that govern observables, while remaining parsimonious in both state dimension and closure complexity. The approach adopted here represents the annulus as a one-dimensional conduit aligned with measured depth, with distributed states that evolve under transient inlet, outlet, and choke conditions [8]. The model is formulated as a balance law with algebraic closures, yielding a differential-algebraic system after spatial discretization. The key design choice is to include a dissolved-gas inventory as an explicit state, so that swelling and release are expressed as mass transfer rather than as ad hoc adjustments to pit volume.

Let $z \in [0, L]$ denote the annular coordinate, with $z = 0$ near the bit and $z = L$ at the surface return. Let $\alpha_g(z,t)$ and $\alpha_l(z,t)$ denote the volumetric fractions of free gas and liquid, with $\alpha_g + \alpha_l = 1$ in the simplest two-phase representation. Let $\rho_g(z,t)$ and $\rho_l(z,t)$ be phase densities, and let $u_g(z,t)$ and $u_l(z,t)$ be phase velocities [9]. A dissolved-gas mass fraction in the liquid, denoted $x_d(z,t)$, is introduced as a scalar field, representing the portion of gas that is not present as a free phase. This dissolved inventory modifies the effective liquid volume

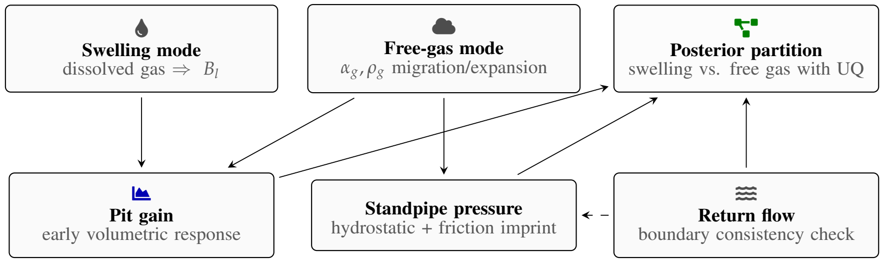

Figure 5 Multi-sensor separation of competing mechanisms: swelling driven by dissolved gas can induce early pit-gain trends, while free-gas holdup and expansion strongly affect both pit gain and pressure transients. Assimilating pit gain together with standpipe pressure and return flow constrains the partition between mechanisms and yields calibrated posterior uncertainty for actionable thresholds.

Table 1 Core elements of the dissolution-aware real-time kick-detection framework

Element	Model representation	Main purpose
Annular transport	1D transient balance laws with dissolved-gas state and MPD boundary conditions	Capture coupled mass, momentum, and phase migration along the wellbore
Dissolution and swelling	Thermodynamic equilibrium map $x_d^\star(p,T)$, swelling factor $B_l(x_d)$, and rate-limited exchange Γ_d	Link pressure/temperature histories to dissolved fraction and mud swelling
Hybrid ROM	Latent state $y(t)$ with constrained operator inference and embedded closures	Provide fast, structure-preserving surrogate for repeated evaluations
Bayesian estimator	Ensemble-based sequential filter in latent space with adaptive inflation	Infer influx parameters and states with quantified uncertainty from streaming data
Numerical experiments	Synthetic well and fluid configurations with controlled scenarios	Assess accuracy, robustness, and computational performance under uncertainty

and can also serve as a buffer that delays free-gas appearance.

The phase-wise mass balances can be written in a conservative form with a source term that transfers mass between free and dissolved forms. A convenient representation places the transfer term in the gas mass equation and couples it to the dissolved fraction equation. One such formulation is

$$\begin{aligned} \partial_t(\alpha_g\rho_g) + \partial_z(\alpha_g\rho_g u_g) &= -\Gamma_d \\ \partial_t(\alpha_l\rho_l) + \partial_z(\alpha_l\rho_l u_l) &= +\Gamma_d \end{aligned} \tag{1}$$

where $\Gamma_d(z,t)$ is the net rate at which free gas dissolves into the liquid minus the rate at which dissolved gas evolves into free gas [10]. A positive Γ_d increases liquid-phase mass and decreases free-gas mass, which is consistent with dissolution. The dissolved inventory is tracked through a transport-reaction equation in the liquid:

$$\partial_t(\alpha_l\rho_l x_d) + \partial_z(\alpha_l\rho_l x_d u_l) = \Gamma_d \tag{2}$$

which guarantees that the sum of free-gas mass and dissolved-gas mass is conserved in the absence of influx and outflow.

The momentum closure can be written in various ways depending on the desired fidelity. For real-time inference, a drift-flux-like closure that captures mixture momentum and relative slip is often adequate [11]. Define the mixture superficial velocity $u_m = \alpha_g u_g + \alpha_l u_l$ and mixture density $\rho_m = \alpha_g\rho_g + \alpha_l\rho_l$. A compressible mixture momentum equation can be written as

$$\partial_t(\rho_m u_m) + \partial_z(\rho_m u_m^2 + p) = -\rho_m g - \partial_z \tau_f \tag{3}$$

where $p(z,t)$ is pressure, g is the gravitational acceleration projected along the well trajectory, and τ_f is a frictional stress term that aggregates wall friction and interfacial effects into an effective pressure gradient. The friction closure is treated as uncertain and is parameterized later so that inference can account for variations in cuttings loading, rheology, and temperature-dependent viscosity changes without overfitting.

To close the system, one must relate ρ_g and ρ_l to p, T, and composition proxies, and one must specify a slip relation to connect u_g and u_l to u_m. The gas density is taken as $\rho_g = \rho_g(p,T)$, which may be computed via a compressibility factor or an equation-of-state mapping [12]. The liquid density is

Table 2 Geometric and flow variables in the annular transport model

Symbol	Description	Units / notes
z	Axial annular coordinate (bit to surface)	m, $z \in [0, L]$
L	Annular length between bit and surface return	m
$u_g(z,t)$	Free-gas axial velocity	m/s
$u_l(z,t)$	Liquid axial velocity	m/s
$u_m(z,t)$	Mixture superficial velocity, $u_m = \alpha_g u_g + \alpha_l u_l$	m/s
$q_k(t)$	Influx mass or volumetric rate at kick depth z_k	Function of time, inference target

Table 3 Thermodynamic and phase-state variables for dissolution-aware modeling

Symbol	Description	Role in model
$p(z,t)$	Pressure along the annulus	Drives solubility, density, and hydrostatics
$T(z,t)$	Temperature field or low-order profile	Affects solubility, density, and viscosity
$\alpha_g(z,t)$	Free-gas volumetric fraction	Governs gas holdup and migration speed
$\alpha_l(z,t)$	Liquid volumetric fraction	Complements α_g; $\alpha_g + \alpha_l = 1$
$x_d(z,t)$	Dissolved-gas mass fraction in liquid	Tracks inventory available for swelling and exsolution
$x_d^\star(p,T)$	Equilibrium dissolved-gas fraction	Tabulated closure for relaxation target
$B_l(x_d)$	Effective liquid swelling factor	Maps dissolution to bulk volume change and density

taken as $\rho_l = \rho_{l,0}(T)/B_l$, where B_l is an effective swelling factor induced by dissolved gas, and $\rho_{l,0}$ is a base density. The swelling factor is modeled as a function of dissolved fraction and thermodynamic state, so that B_l increases when dissolution increases. The slip relation is written as

$$u_g - u_l = S(\alpha_g, p, T; \theta_s) \tag{4}$$

where S is a slip function with parameters θ_s that can be inferred or fixed. The intent is not to perfectly model micro-scale hydrodynamics, but to represent the leading-order consequence that free gas migrates upward relative to the liquid, thereby shaping the timing of surface signals.

Boundary conditions depend on the operational mode [13]. At the bit, influx is represented as a source of gas mass added at a depth $z = z_k$ with a rate $q_k(t)$ that can be time-varying. The influx can be expressed as an addition to the gas mass equation localized in space, and the rate becomes a primary inference target. At the surface, the choke imposes a relation between flow-out, backpressure, and downstream conditions. A simplified boundary condition can be written as

$$p(L,t) = p_c(t) + \Delta p_\chi(q_{\text{out}}(t)) \tag{5}$$

where $p_c(t)$ is the applied casing pressure or choke set-point and Δp_χ is a choke pressure drop function of outflow. The sensor map includes measurements such as pit-volume change $\Delta V_p(t)$, standpipe pressure, and return flow rate. Pit-volume change is expressed as an integral of net volumetric imbalance between inflow and outflow, but in dissolution-aware modeling it is also influenced by swelling of the liquid phase because swelling changes the effective bulk volume for a given mass [14]. The model therefore links pit gain to both boundary fluxes and internal thermodynamic state.

Table 4 Balance laws and source terms in the annular transport formulation

Equation	Representative term	Physical meaning
Gas mass	$\partial_t(\alpha_g\rho_g) + \partial_z(\alpha_g\rho_g u_g) = -\Gamma_d$	Free gas is advected and reduced by dissolution
Liquid mass	$\partial_t(\alpha_l\rho_l) + \partial_z(\alpha_l\rho_l u_l) = +\Gamma_d$	Liquid gains mass from dissolved gas
Dissolved inventory	$\partial_t(\alpha_l\rho_l x_d) + \partial_z(\alpha_l\rho_l x_d u_l) = \Gamma_d$	Conserves total gas between free and dissolved forms
Mixture momentum	$\partial_t(\rho_m u_m) + \partial_z(\rho_m u_m^2 + p) = -\rho_m g - \partial_z\tau_f$	Compressible momentum balance with gravity and friction
Mass transfer	$\Gamma_d = \kappa_d(x_d^\star - x_d)\alpha_l\rho_l$	Relaxation toward thermodynamic equilibrium at rate κ_d

Table 5 Dissolution and swelling closure parameters

Parameter	Description	Role in closure
κ_d	Effective mass-transfer rate for dissolution/exsolution	Controls relaxation time scale between x_d and $x_d^\star$
β_1	Linear swelling coefficient in $B_l = 1 + \beta_1 x_d + \beta_2 x_d^2$	Governs first-order volumetric response to dissolved gas
β_2	Quadratic swelling coefficient	Captures nonlinear saturation of swelling at high x_d
$\rho_{l,0}(T)$	Base liquid density without dissolved gas	Reference for computing swollen liquid density ρ_l
M_g	Effective gas molar mass	Enters real-gas density $\rho_g = pM_g/(ZRT)$
$Z(p,T)$	Compressibility factor from EOS table	Encodes deviation from ideal-gas behavior over HPHT range

The resulting system is a coupled set of nonlinear balance laws with algebraic closures. For inference, it is essential to represent both process noise and parametric uncertainty. Process noise accounts for unmodeled disturbances such as intermittent cuttings beds, sensor latency, and short-term valve dynamics. Parametric uncertainty accounts for imperfect friction and property closures [15]. Rather than treat uncertainty as additive white noise on outputs, the framework embeds uncertainty in selected parameters that directly influence observables, so that posterior uncertainty can be interpreted physically.

An additional complication is temperature variation. A full thermal model can be expensive and often under-observed. The approach adopted here treats temperature $T(z,t)$ as a low-dimensional field represented by an affine-in-time profile that is updated from operational measurements or from a simple relaxation model toward known geothermal and circulation conditions. This avoids introducing an additional PDE while still enabling the dissolution closure to respond to temperature changes that materially affect solubility and density.

Finally, the model must remain numerically robust under the aggressive time steps demanded by real-time assimilation [16]. Hyperbolic balance laws can develop sharp gradients during kick migration, and phase fractions must remain within $[0,1]$. The discretization is therefore designed to be conservative, to preserve positivity, and to avoid spurious oscillations. These properties are later reflected in the reduced-order representation so that the reduced model does not violate the constraints that keep the full model physically plausible.

3. Thermodynamic Dissolution and Swelling Closure

The distinguishing feature of dissolution-aware kick inference is that dissolved gas is modeled as a thermodynamic state constrained by phase equilibrium rather than as an empirical correction. The closure must supply two pieces of information: an equilibrium or quasi-equilibrium mapping from pressure and

Table 6 Design features of the hybrid reduced-order surrogate

Aspect	Full-order representation	Reduced representation
State dimension	$x(t) \in \mathbb{R}^N$ with grid-resolved fields	Latent $y(t) \in \mathbb{R}^r$, $r \ll N$
State coordinates	Direct physical variables on grid	Transformed coordinates (log-densities, logits for fractions) decoded to physical space
Dynamics	PDE discretization and implicit/-explicit time stepping	Time-discrete map $y_{n+1} = Ay_n + Bu_n + c + \mathcal{N}(y_n, u_n)$ via operator inference
Thermodynamics	Online EOS solves or table lookup	Embedded differentiable lookup tables for $x_d^\star$ and $Z(p, T)$
Constraints	Conservation and positivity from numerical scheme	Enforced via parameter constraints, coordinate transforms, and mass functional matching

temperature to dissolved fraction, and a volumetric response mapping from dissolved fraction to liquid swelling and effective density [17]. In addition, a dynamic mass-transfer term Γ_d must relate the current dissolved fraction to its equilibrium target, because dissolution and exsolution may be rate-limited by mixing and interfacial area rather than instantaneous.

A common equilibrium viewpoint is to treat gas solubility as the solution to a fugacity equality between phases. For real-time modeling, the aim is not to compute full composition speciation but to compute an effective dissolved fraction that captures the leading-order swelling behavior. This can be done by introducing an equilibrium dissolved mass fraction $x_d^\star(p, T)$ obtained from an equation-of-state calculation for a representative gas component proxy and a representative liquid proxy. The mapping is tabulated offline across the pressure and temperature range of interest, and online the model interpolates this tabulation. The tabulation approach is attractive because it converts an iterative thermodynamic solve into a fast lookup, while still preserving the thermodynamic trend structure that empirical correlations may not generalize [18].

Dynamic exchange is represented by a relaxation-to-equilibrium model,

$$\Gamma_d = \kappa_d \big(x_d^\star(p, T) - x_d\big)\alpha_l \rho_l \tag{6}$$

where κ_d is an effective mass-transfer rate parameter that aggregates interfacial area and mixing. This parameter can be treated as uncertain, and in some cases it can be inferred from data when sufficient excitation exists. The relaxation form ensures that Γ_d vanishes when x_d equals its equilibrium value and drives the dissolved fraction toward equilibrium otherwise. To ensure that x_d remains in a physically meaningful range, a bounded coordinate transformation is used in the numerical implementation, as discussed later in the reduced-order section [19].

Swelling is represented through a factor B_l that modifies the liquid specific volume. Let $v_{l,0}(T)$ be the base liquid specific volume. Define the swollen specific volume as $v_l = B_l v_{l,0}$. The swelling factor is modeled as a function of dissolved fraction and state:

$$B_l = 1 + \beta_1 x_d + \beta_2 x_d^2 \tag{7}$$

where coefficients β_1 and β_2 are calibrated from thermodynamic computations or from fluid-lab data when available. The quadratic form is chosen to flexibly capture diminishing returns in swelling at higher dissolved fractions while remaining simple enough for inference. The coefficients are treated as uncertain within bounds consistent with the expected fluid system. The swollen liquid density is then [20]

$$\rho_l = \frac{\rho_{l,0}(T)}{B_l} \tag{8}$$

which ensures that increasing swelling reduces density in a manner consistent with increased specific volume.

A crucial numerical issue is that swelling interacts with pit gain through volumetric accounting. Pit volume is a surface tank measurement that reflects both net inflow-outflow imbalance and the bulk volume of fluid returning, which in turn depends on density and swelling. In the model, the instantaneous bulk volumetric flow of liquid at the surface is computed from mass flow and density, so swelling modifies the relationship between mass flux and volumetric flow. This provides a pathway by which dissolution can generate pit gain without requiring large free-gas volumes, which is one of the reasons dissolution-aware modeling improves interpretability in early-stage kicks [21].

The closure must also connect to gas density and compressibility. The free gas phase is modeled as a real gas with density $\rho_g(p, T)$. For computational tractability, the mapping from (p, T) to ρ_g is expressed through a compressibility factor function $Z(p, T)$:

$$\rho_g = \frac{pM_g}{Z(p, T)RT} \tag{9}$$

Table 7 Bayesian inversion ingredients in latent space

Quantity	Symbol	Treatment in inference
Latent state	y_n	Propagated by ROM with process noise, updated by ensemble analysis
Parameters	θ	Included as augmented state with bounded random-walk dynamics
Influx profile	Subset of θ (e.g. rate, depth, onset time)	Low-dimensional parameterization targeted by posterior
Process noise	w_n	Represents model discrepancy and unresolved disturbances
Observation noise	v_n	Encodes sensor error statistics and innovation weighting
Sensor bias	Included in θ	Estimated jointly to avoid misattributing offsets to influx
Inflation factor	User-controlled hyperparameter	Adjusts ensemble spread to prevent collapse under mismatch

where M_g is an effective molar mass and R is the universal gas constant. The function Z can be computed from an equation-of-state model offline and tabulated similarly to solubility. This strategy decouples online performance from the complexity of the thermodynamic model while keeping the response consistent with compressible behavior [22]. The effective molar mass can be treated as a nuisance parameter that absorbs composition uncertainty when the actual gas composition is not known in real time.

The above closure provides equilibrium behavior and swelling response, but it remains to ensure that the combined PDE-closure system does not become numerically stiff. Stiffness arises when κ_d is large relative to the transport time scales, causing rapid relaxation that requires small time steps for explicit schemes. The framework addresses this by using an implicit update for the dissolved fraction reaction term, while keeping transport explicit or semi-implicit. For example, after a transport update yields an intermediate dissolved fraction $\tilde{x}_d$, the reaction update solves

$$x_d^{n+1} = \tilde{x}_d + \Delta t\, \kappa_d \left(x_d^{\star} - x_d^{n+1}\right) \tag{10}$$

which can be rearranged into a closed-form expression: [23]

$$x_d^{n+1} = \frac{\tilde{x}_d + \Delta t\, \kappa_d x_d^{\star}}{1 + \Delta t\, \kappa_d} \tag{11}$$

This update is unconditionally stable for the reaction term and preserves bounds when combined with a bounded representation of $x_d^{\star}$.

A further consistency requirement is that the dissolution inventory and swelling do not violate overall mass conservation. Because swelling changes volume but not mass, conservation is preserved as long as the mass equations remain conservative and the volume is computed from mass and density. The model therefore uses mass as the fundamental conserved quantity, and it computes volume diagnostically. This design choice prevents spurious creation of mass that could otherwise occur if swelling were implemented as a direct volumetric expansion without corresponding density adjustment.

The equilibrium mapping $x_d^{\star}(p, T)$ can be computed by various thermodynamic approaches [24]. The present paper does not require a specific choice, but it assumes the mapping is monotone increasing in pressure at fixed temperature for the relevant regime and decreasing in temperature at fixed pressure, consistent with typical solubility trends. The essential modeling issue is not the precise thermodynamic model, but the integration of the equilibrium mapping into a dynamical inference system with uncertainty. In that respect, Manikonda et al. (2021) provided an early mechanistic kick model in which a thermodynamic solubility approach is coupled to kick migration in synthetic-based mud [25], using phase-equilibrium concepts to estimate dissolved gas and mud swelling as part of a computationally efficient simulator. The present work takes the complementary step of embedding a similar class of dissolution-aware closure into a structure-preserving reduced-order and Bayesian inversion pipeline suitable for continuous online assimilation, with explicit uncertainty propagation [26].

4. Structure-Preserving Hybrid Reduced-Order Surrogate

Real-time Bayesian inference requires repeated forward model evaluation. Even modest spatial discretizations of the coupled balance laws can produce state dimensions that are too large for

Table 8 Numerical experiment scenarios and evaluation focus

Scenario	Main focus	Key variations	Primary metrics
Dissolution vs. none	Role of swelling in pit gain	Solubility strength, swelling coefficients	Pit-gain timing, inferred free-gas holdup, posterior separation of mechanisms
Operational transients	Robustness to pump and choke changes	Pump ramps, backpressure steps, non-kick disturbances	False-alarm rate, correct attribution to boundary actions
Property uncertainty	Impact of correlation errors	Gas density/viscosity and swelling-model perturbations	Bias in inferred influx, credible-interval coverage
Mass-transfer rate	Identifiability of κ_d	Slow vs. fast dissolution regimes	Posterior spread on κ_d, fit to swelling dynamics
Computational performance	Real-time suitability of ROM	Ensemble size, time step, rollout length	Speedup over full model, latency per assimilation cycle

ensemble propagation or for gradient-based optimization under tight time budgets. A reduced-order model (ROM) is therefore constructed, but the ROM must be carefully designed. Standard projection-based ROMs can struggle with shocks, phase fraction constraints, and strongly nonlinear closures; purely data-driven ROMs can violate conservation, lose stability outside the training set, and produce unphysical negative densities. The approach in this paper is a hybrid ROM that combines a low-dimensional latent representation with an operator-inferred dynamical update that is constrained to preserve key invariants and inequality constraints.

The full discretized state at time t is denoted $x(t) \in \mathbb{R}^N$, containing fields such as α_g, ρ_g, ρ_l, u_m, and x_d across grid cells. The ROM introduces a latent coordinate $y(t) \in \mathbb{R}^r$ with $r \ll N$ and a decoder map $D : \mathbb{R}^r \to \mathbb{R}^N$ such that $x \approx D(y)$. The decoder is chosen to be affine in conserved variables and nonlinear only in variables that require bound enforcement [27]. In particular, phase fractions and dissolved fractions are represented through logit-like transforms to enforce bounds. For example, the dissolved fraction is represented as

$$x_d = \sigma(\eta_d) \tag{12}$$

with $\sigma(\cdot)$ a sigmoid map and η_d an unconstrained coordinate, which prevents the ROM from producing negative or greater-than-one dissolved fractions. Similar transforms can be used for α_g. Densities are represented in logarithmic coordinates to enforce positivity: [28]

$$\rho_g = \exp(\xi_g), \quad \rho_l = \exp(\xi_l) \tag{13}$$

These transforms convert inequality constraints into unconstrained coordinates, making it easier to build stable reduced dynamics.

The temporal evolution of the latent state is represented by an operator-inference model that approximates the time-discrete flow map. Let $\Phi_{\Delta t}$ denote the full-model update over a time step Δt. The ROM approximates

$$y_{n+1} \approx F(y_n, u_n) \tag{14}$$

where u_n denotes known inputs such as pump rate and choke set-point. The function F is not a black-box neural network; it is constructed as a constrained polynomial and rational operator designed to preserve a discrete analog of mass conservation and to maintain dissipativity in a chosen energy-like norm. One practical form is [29]

$$y_{n+1} = Ay_n + Bu_n + c + \mathcal{N}(y_n, u_n) \tag{15}$$

where $\mathcal{N}$ is a nonlinear term represented in a basis of low-order monomials and selected interaction terms that mirror the physical nonlinearities, such as products of phase fraction and velocity. The coefficients of A, B, c, and $\mathcal{N}$ are learned from full-model trajectory data generated offline under a range of scenarios that span plausible operating conditions.

The central innovation is to impose constraints on the learned operator so that it preserves invariants. Global mass conservation can be expressed as a linear functional of the decoded state. Let $m(x)$ denote the total mass in the annulus plus pits, and let m be approximated as $m(D(y))$. Conservation in the absence of boundary fluxes implies

$$m(D(y_{n+1})) - m(D(y_n)) = 0 \tag{16}$$

which can be enforced approximately by constraining the ROM coefficients so that the decoded update lies in the nullspace of the mass functional for interior dynamics [30]. In practice,

Table 9 Sensor set and their roles in dissolution-aware kick inference

Sensor	Observable	Characteristics	Role in inference
Pit-volume system	Pit gain $\Delta V_p(t)$	Integrating, subject to calibration bias	Primary indicator of volumetric imbalance and swelling effects
Standpipe pressure	Circulation pressure at surface	High-frequency, sensitive to friction and hydrostatics	Helps distinguish property errors from influx-induced pressure changes
Return-flow meter	Flow-out rate at surface	Directly affected by swelling and multiphase migration	Constrains timing and magnitude of returning gas/liquid mixture
Choke pressure	Upstream/downstream choke pressures	Influenced by MPD control actions	Links boundary actuation to observed transients and pressure drops
Temperature estimate	Low-order $T(z,t)$ profile or proxy	Slowly varying, often under-observed	Feeds solubility and density closures for dissolution modeling

because boundary fluxes exist, the conservation constraint is enforced on the residual after accounting for known boundary contributions. This yields linear equality constraints on the ROM parameters that can be incorporated into a constrained least-squares fit.

Stability is addressed by enforcing a discrete dissipativity condition. Define an energy-like quadratic form $E(y) = \frac{1}{2}y^\top Py$ with $P \succ 0$. A sufficient condition for stability of the linear part is that $A^\top PA - P \preceq -Q$ for some $Q \succeq 0$. This can be imposed as a semidefinite constraint in the learning step or approximated by penalizing violations [31]. For the nonlinear part, local Lipschitz bounds are enforced by restricting coefficient magnitudes and by training on trajectories that include aggressive transients, so that the learned operator does not extrapolate into unstable regimes. While this does not provide a global proof for the full nonlinear ROM, it yields a practically robust surrogate that does not exhibit spurious blow-up under time steps needed for real-time use.

Because the thermodynamic closure can be represented through tabulated functions, the ROM includes these closures as embedded differentiable components rather than learning them from scratch. Specifically, given a decoded pressure and temperature field, the ROM computes $x_d^\star(p,T)$ and $Z(p,T)$ by interpolation. These interpolations are differentiable and fast, and they preserve monotonicity when monotone interpolation schemes are used [32]. The mass-transfer update for x_d is also embedded in the ROM, using the unconditionally stable implicit reaction update described earlier. This hybrid design reduces data requirements and improves generalization because the ROM does not need to infer thermodynamic trends solely from limited training data.

The offline training data is generated from the full model by sampling across influx depth, influx rate profiles, pump rates, choke settings, base mud properties, and temperature profiles. Scenarios include both true kicks and non-kick transients such as pump ramps and choke perturbations so that the ROM learns to distinguish them. The training objective minimizes mismatch between full-model decoded states and ROM predictions over multi-step rollouts rather than one-step errors alone. This is important because one-step errors can cancel, yet multi-step rollouts can drift into unphysical regimes if the operator is not well learned [33]. The rollout loss is combined with constraint penalties for mass conservation and with regularization that discourages overly complex nonlinear terms.

A practical ROM must also provide a linearized sensitivity model to support Bayesian filtering. Because the ROM is differentiable, Jacobians can be computed analytically from the polynomial operator and the decoder transforms. This yields consistent local linearizations used in covariance propagation. In addition, ensemble propagation can be done cheaply because each ROM evaluation is a low-dimensional update [34]. The combination of cheap evaluation and consistent linearization is essential for online estimation in which multiple hypotheses must be propagated to represent uncertainty.

The ROM is validated by comparing its predictions against the full model across a held-out scenario set. Validation focuses on outputs that drive inference, such as pit gain, standpipe pressure, and surface return flow, rather than only on internal fields. The ROM is also stress-tested by extrapolating to slightly beyond the training set in pressure and temperature, but within physically plausible ranges. The constraint enforcement and embedded thermodynamic closures are crucial in this regime, because they prevent the ROM from producing impossible phase fractions or negative densities when confronted with unfamiliar combinations of inputs.

5. Bayesian Inversion and Online Assimilation

The purpose of the reduced model is not merely to forecast, but to infer hidden kick parameters from noisy surface measurements and to quantify the uncertainty of those inferences [35]. The inference problem is naturally posed in a Bayesian framework because the system is stochastic, under-observed, and subject to model discrepancy. The latent state $y(t)$ evolves according to the ROM dynamics, while the observations $d(t)$ are generated from a measurement map applied to the decoded state, corrupted by noise and bias. The inference targets include both dynamic quantities, such as the latent state and dissolved fraction distribution, and static or slowly varying parameters, such as friction multipliers, mass-transfer rate κ_d, and influx rate profile parameters.

Let y_n denote the latent state at discrete time t_n, and let θ denote a vector of parameters. The ROM dynamics define a transition density [36]

$$y_{n+1} = F(y_n, u_n; \theta) + w_n \tag{17}$$

where w_n is process noise representing unresolved disturbances and ROM discrepancy. Observations are modeled as

$$d_n = H(D(y_n), u_n; \theta) + v_n \tag{18}$$

where H is a sensor map producing pit gain increments, standpipe pressure, and return flow, and v_n is observation noise. The sensor map includes integration of volumetric flow to produce pit gain, and it includes optional lag models to represent transport delay in surface instrumentation. Because the ROM is differentiable, H can be linearized around the current estimate, which is useful for covariance updates.

A central modeling choice is how to represent the influx [37]. Rather than represent influx as an arbitrary function of time and depth, which would be unidentifiable from sparse measurements, the framework parameterizes influx by a small set of interpretable parameters. One representation uses a depth location z_k, an onset time t_k, and a rate profile described by a piecewise-smooth function with a small number of coefficients. These coefficients become part of θ and can be estimated. The parameterization is chosen to be flexible enough to represent gradual influx ramp-up as well as abrupt kicks, while remaining identifiable given the measurement set.

The posterior distribution of interest is $p(y_{0:n}, \theta \mid d_{0:n})$. Exact inference is intractable due to nonlinearity, but approximate sequential methods are effective [38]. The paper adopts an ensemble-based sequential Bayesian filter operating on the ROM. The ensemble represents a set of particles $\{(y_n^{(i)}, \theta^{(i)})\}_{i=1}^{M}$ propagated by the ROM with stochastic perturbations. At each observation time, the ensemble is updated using a Kalman-like analysis step based on sample covariances. This yields an ensemble Kalman filter variant that is computationally efficient and robust to moderate nonlinearity.

Because the system can be strongly nonlinear during rapid gas expansion, and because measurement errors can be correlated, the filter incorporates covariance inflation and localization in the latent space. Inflation prevents ensemble collapse by increasing variance when model mismatch is detected. Localization reduces spurious correlations that can arise when M is small relative to the effective dimension [39]. In the latent space, localization is implemented by damping cross-covariances between latent modes that have weak physical coupling, as inferred from training statistics. This is not an arbitrary tuning device; it reflects the fact that the latent coordinates are constructed to have approximate physical meaning through the decoder structure, so correlation patterns can be interpreted and constrained.

Parameter estimation is handled by augmenting the state with parameters or by using a dual-estimation scheme. In state augmentation, parameters are treated as random-walk states:

$$\theta_{n+1} = \theta_n + \epsilon_n \tag{19}$$

with small ϵ_n to represent slow variation [40]. The augmented state is then filtered together with y_n. This approach is simple and works well when parameters influence outputs sufficiently. However, it can suffer from identifiability issues if multiple parameter combinations explain the same outputs. The framework therefore uses informative priors and constrains parameters to physically plausible ranges. For instance, friction multipliers are bounded around unity, and κ_d is bounded to reflect plausible mixing time scales.

Identifiability is analyzed by examining the sensitivity of outputs to parameters and to key latent coordinates [41]. Because the ROM is differentiable, local sensitivities can be computed efficiently. If pit gain, standpipe pressure, and return flow are simultaneously used, the inference becomes better conditioned than if pit gain alone is used. Pit gain is sensitive to both swelling and free-gas volume, while pressure is sensitive to hydrostatic distribution and friction. The joint use of pressure and flow data thus helps separate dissolution-driven swelling from free-gas expansion, particularly when managed pressure drilling boundary conditions impose backpressure transients that would otherwise confound interpretation.

A critical feature of the Bayesian approach is the ability to produce posterior predictive distributions for quantities of interest [42]. For decision support, the relevant quantity is often the probability that influx exceeds a threshold or that a free-gas volume at surface will exceed a manageable limit within a time window. These probabilities can be computed by propagating the ensemble forward under candidate control actions. Because the ROM is fast, multiple what-if rollouts can be evaluated in real time, enabling risk-informed control adjustments.

The framework also accounts for the fact that sensors may be biased or delayed. Bias terms can be included in θ, and delay can be modeled as a first-order lag. Including these terms prevents the filter from misattributing systematic measurement discrepancies to physical influx [43]. Bias estimation is particularly important for pit volume measurements, where tank calibration errors can produce persistent offsets. When bias is accounted for, the posterior on influx rate becomes less sensitive to such offsets and more driven by dynamic consistency across multiple sensors.

The assimilation scheme is validated by synthetic experiments in which the full model generates measurement streams with injected noise and bias. The filter uses the ROM, not the full model, to perform inference. Performance is evaluated by comparing posterior means and credible intervals to ground truth, by assessing how quickly the filter detects influx onset, and by measuring false alarm rates under non-kick transients [44]. The numerical section reports these evaluations and highlights scenarios in which dissolution plays a decisive role in early detection.

6. Numerical Experiments and Sensitivity Analysis

The numerical evaluation is designed to test not only accuracy but also robustness under uncertainty and under confounding operational transients. Because field data is heterogeneous and often proprietary, the experiments use a simulated well and fluid system with parameters chosen to be representative of oil-based and synthetic-based mud operations. The full model provides a high-fidelity baseline, and the reduced model is trained on a scenario ensemble sampled across operating ranges. The Bayesian filter then operates purely on reduced-model dynamics, using simulated sensor streams derived from the full model with added noise, bias, and delay.

The primary well configuration includes a vertical or mildly deviated annulus of length L, with a representative hydraulic diameter and roughness [45]. Pump rate schedules include steady circulation, ramp-up, and ramp-down transients. Choke schedules include step changes in backpressure and smooth adjustments. Kick scenarios include shallow and deep influx points, with both abrupt and gradual rate profiles. Dissolution strength is varied by scaling the equilibrium dissolved fraction mapping and swelling coefficients, representing different mud formulations and gas solubility characteristics. This variability is essential because the inference system must function across fluid systems, not only for a single tuned case [46].

Outputs include pit gain, standpipe pressure, return flow, and computed choke pressure drop. Noise is modeled as Gaussian with sensor-specific variances, and bias is modeled as a slowly varying offset. In addition, short bursts of outlier noise are injected to simulate sensor glitches. The filter is tested both with and without outlier-robust modifications. The focus is on the baseline filter described earlier; outlier robustness is implemented by inflating observation noise when innovations exceed a threshold, which reduces the impact of rare spikes without requiring explicit heavy-tailed likelihoods.

The first set of experiments isolates dissolution effects [47]. Two scenarios are compared: one with significant solubility leading to swelling, and one with negligible dissolution. Both scenarios have identical influx mass rates at the kick depth. In the negligible-dissolution case, pit gain is dominated by free-gas expansion and arrives at the surface later due to migration. In the significant-dissolution case, pit gain begins earlier because swelling increases the return flow volume even when free gas is largely dissolved. The dissolution-aware model reproduces this early pit-gain onset, while a dissolution-ignorant model interprets the same pit gain as free-gas presence and consequently overestimates free-gas holdup [48]. In the Bayesian setting, this misinterpretation manifests as a posterior that places excessive probability on high free-gas volume near the top of the annulus, which then leads to overly conservative control recommendations. By contrast, the dissolution-aware inference yields posterior mass concentrated on increased dissolved fraction and moderate free-gas holdup, aligning better with the ground truth.

The second set of experiments examines confounding operational transients. A pump-rate ramp down produces a pit gain signature because reduced circulation changes return flow and pressure drop. A choke backpressure increase produces a pressure transient that can resemble the initial pressure response of an influx. The inference system must avoid false alarms in these cases [49]. When only pit gain is assimilated, the filter is susceptible to false positives because pit gain is not uniquely informative. When pit gain is combined with pressure and flow-out, the posterior correctly attributes the observed changes to boundary conditions rather than to influx. This highlights the importance of multi-sensor assimilation and the advantage of a state-space model that can represent both operational and kick-induced changes consistently.

The third set of experiments explores property-model uncertainty. Gas density and viscosity influence hydrostatic and frictional pressure gradients, and swelling influences volumetric return [50]. The filter is run with uncertain property parameters drawn from prior distributions. In some runs, the true property behavior differs from the prior mean by a few percent in key regions, consistent with the magnitude of correlation errors observed in practice. The results show that small property mismatches can bias inferred influx rates if they are not modeled as uncertainty. When the filter includes these uncertainties, posterior intervals widen appropriately and mean estimates shift toward the truth. Importantly, credible intervals provide a quantification of ambiguity that can be used operationally. For example, if the posterior probability of a nonzero influx remains low despite pit gain, the system can recommend continued monitoring rather than immediate shut-in [51]. Conversely, when multiple sensors coherently indicate an influx, the posterior concentrates quickly and triggers a high-probability alert.

The fourth set of experiments studies computational performance. The ROM evaluation time is compared to the full model for a representative spatial resolution. The ROM achieves orders-of-magnitude speedup, enabling ensemble sizes sufficient for uncertainty quantification. The differentiability of the ROM also enables computation of sensitivity metrics at negligible additional cost [52]. This supports diagnostic checks such as determining which sensors currently provide the most information about influx rate. In operational terms, such information can guide sensor validation and can indicate when a sensor failure may significantly degrade inference quality.

The fifth set of experiments evaluates the impact of mass-transfer rate κ_d. When κ_d is large, dissolved fraction tracks equilibrium closely, and swelling responds rapidly to pressure changes. When κ_d is small, dissolution is slow, and free gas persists more strongly. These regimes have distinct signatures [53]. The filter can estimate κ_d when the data includes pressure variations that excite dissolution dynamics. When pressure is nearly steady, κ_d becomes weakly identifiable, and its posterior remains close to the prior. The system is designed to handle this by not forcing overconfident parameter estimates; instead, it propagates uncertainty and reflects it in predictions. This behavior is critical because overconfident but wrong estimates of mass-transfer dynamics could lead to systematic misinterpretation of pit gain during subsequent events.

Across the numerical suite, the dissolution-aware framework demonstrates improved separation between swelling-induced and free-gas-induced pit gain, reduced false alarms under operational transients, and coherent uncertainty quantification under property mismatch [54]. The results also highlight limitations. When sensors are sparse and operational excitation is minimal, some parameters remain weakly identifiable, and posterior uncertainty remains large. This is not a failure of the method but a reflection of information limits. The appropriate response is to design operational tests or control perturbations that increase identifiability when safe and feasible, rather than to rely on inference alone.

7. Conclusion

This paper developed a dissolution-aware modeling and inference framework for real-time gas-kick detection under managed pressure drilling. The central premise is that pit gain, pressure, and flow signals are shaped by a coupled set of mechanisms that include not only free-gas migration and compressibility but also dissolution into the drilling fluid and the resulting swelling of the liquid phase [55]. A coupled annular transport model was formulated with an explicit dissolved-gas inventory and a thermodynamic closure that maps pressure and temperature to equilibrium dissolved fraction and swelling, supplemented by a rate-limited mass-transfer term. The model was then reduced through a structure-preserving hybrid reduced-order approach that enforces positivity and conservation while embedding thermodynamic lookups as differentiable components. This reduced model enabled online Bayesian assimilation via an ensemble-based sequential method that estimates both hidden states and key parameters while propagating uncertainty into operationally relevant risk metrics.

The numerical experiments demonstrated that dissolution-aware inference can distinguish early swelling-driven pit gain from later free-gas expansion in regimes where dissolution-ignorant approaches tend to overestimate free-gas holdup. The experiments also showed that multi-sensor assimilation reduces false alarms under operational transients and that explicit modeling of property uncertainty prevents biased estimates when fluid-property correlations deviate by a few percent [56]. The framework is designed to remain computationally feasible for continuous deployment, supporting ensemble-based uncertainty quantification and forward what-if rollouts for decision support.

Several extensions are natural. The thermodynamic mapping can be enriched to include multi-component gas proxies when composition measurements become available, and the thermal representation can be upgraded to a low-order energy balance when temperature variation is strongly coupled to solubility. The slip and friction closures can be refined with additional state dependence while retaining the constraint structure that preserves stability. Finally, field deployment will require systematic handling of sensor validation, data latency, and operational constraints. The methods presented here provide a foundation for such deployment by unifying dissolution-aware physics, structure-preserving reduction, and Bayesian inference into a coherent real-time architecture [57].

Acknowledgments

We would like to thank the reviewers of this research for their helpful comments and suggestions.

References

[1] A. Adams and S. Glover, “An investigation into the application of qra in casing design,” in *SPE Applied Technology Workshop on Risk Based Design of Well Casing and Tubing*, SPE, 5 1998.

[2] K. Manikonda, A. R. Hasan, O. Kaldirim, N. Rahmani, and M. A. Rahman, “Estimating swelling in oil-based mud due to gas kick dissolution,” in *International conference on offshore mechanics and arctic engineering*, vol. 84430, p. V011T11A039, American Society of Mechanical Engineers, 2020.

[3] A. K. Sleiti, W. A. Al-Ammari, M. Abdelrazeq, M. El-Naas, M. A. Rahman, A. Barooah, R. Hasan, and K. Manikonda, “Comprehensive assessment and evaluation of correlations for gas-oil ratio, oil formation volume factor, gas viscosity, and gas density utilized in gas kick detection,” *Journal of Petroleum Science and Engineering*, vol. 207, p. 109135, 2021.

[4] W. Ren, H. Fan, S. Deng, C. Cui, Q. Peng, X. Liu, and X. Dou, “Displacement calculation of dynamic killing drilling in deepwater,” in *SPE Nigeria Annual International Conference and Exhibition*, SPE, 8 2015.

[5] X. Li, C. Guan, X. Sui, and . Gangtao, “A new approach for early gas kick detection,” in *SPE International Oil and Gas Conference and Exhibition in China*, SPE, 11 1998.

[6] F. Kesuma, “Pengaruh kick off point terhadap perencanaan lintasan pemboran berarah pada sumur w, x, y, z,” 4 2016.

[7] P. M. Syamlal, “Development of technologies and analytical capabilities for vision 21 energy plants,” 4 2001.

[8] L. Wanying, L. Ying, H. Guisheng, F. Jianhong, P. Yong, C. Yuhai, and S. Ambrish, “A dynamic simulation of annular multiphase flow during deep-water horizontal well drilling and the analysis of influential factors,” 1 2016.

[9] G. Zhou and A. Prosperetti, “Violent expansion of a rising taylor bubble,” *Bulletin of the American Physical Society*, 11 2019.

[10] N. S. Noori, T. I. Waag, H. Viumdal, R. Sharma, M. H. Jondahl, and A. Jinasena, "Non-newtonian fluid flow measurement in open venturi channel using shallow neural network time series and non-contact level measurement radar sensors," in *SPE Norway Subsurface Conference*, SPE, 11 2020.

[11] G. Z. Han, L. Lemesany, A. A. Azizov, and F. DeLeon, "Practical directional drilling techniques in pinedale field wyoming to improve drilling performance," in *SPE Unconventional Resources Conference Canada*, SPE, 11 2013.

[12] S. Q. Tunio, A. H. Tunio, N. A. Ghirano, and S. Irawan, "Is it possible to ignore problems rising during vertical drilling? a review," 11 2011.

[13] A. Hamid, "Evaluasi penanggulangan kick menggunakan metode driller, wait & weight, dan concurrent pada sumur x lapangan y," *PETRO:Jurnal Ilmiah Teknik Perminyakan*, vol. 2, 8 2015.

[14] D. L. Kirchman, *Dead Zones*. Oxford University PressNew York, 2 2021.

[15] Z. Lippai, Z. Frei, and Z. Haiman, "Prompt shocks in the gas disk around a recoiling supermassive black hole binary," *The Astrophysical Journal*, vol. 676, pp. L5–L8, 3 2008.

[16] E. Saeverhagen, C. Erichsen, A. K. Nesheim, and G. Waldron, "3d rss for 24-in. section sets inclination record on the grane field by introduction of an integrated drilling and surveying bottomhole assembly," in *SPE Annual Technical Conference and Exhibition*, SPE, 9 2008.

[17] "Well control," 4 2018.

[18] W. Guo, H. Zhou, H. Fan, N. Si, J. Liu, D. Ma, and W. Pang, "Utilising managed pressure drilling to drill shale gas horizontal well in fuling shale gas field," in *SPE Asia Pacific Oil & Gas Conference and Exhibition*, SPE, 10 2016.

[19] F. Di, P. Baraldi, L. Brivio, E. Zio, and C. Magno, *Resistance-based probabilistic design by order statistics for an oil and gas deep-water well casing string affected by wear during kick load*, pp. 750–757. CRC Press, 9 2016.

[20] N. M. Dinh, "Early kick detection using data-driven bayesian network: model development and experimental testing," 5 2020.

[21] S. Krueger, K. Gray, and D. Killip, "Fifteen years of successful coiled tubing re-entry drilling projects in the middle east - driving efficiency and economics in maturing gas fields," in *SPE/IADC Middle East Drilling Technology Conference & Exhibition*, SPE, 10 2013.

[22] D. C. Marques, P. Ribeiro, O. Santos, and R. F. T. Lomba, "Thermodynamic behavior of olefin/methane mixtures applied to synthetic-drilling-fluid well control," *SPE Drilling & Completion*, vol. 33, pp. 230–240, 8 2018.

[23] B. T. H. Marbun and A. M. I. Shidiq, "Estimation of annulus pressure fluids kick for vertical well using moore method and integrated numerical simulation," in *North Africa Technical Conference and Exhibition*, SPE, 4 2013.

[24] A. Khalid, Q. Ashraf, K. Luqman, A. Hadj-Moussa, D. Sheikh, and S. Zafar, "Reaching target depth with zero npt in an hpht tight gas well: A case for automated managed pressure drilling," in *Abu Dhabi International Petroleum Exhibition & Conference*, SPE, 11 2019.

[25] K. Manikonda, A. R. Hasan, N. H. Rahmani, O. Kaldirim, C. E. Obi, J. J. Schubert, and M. A. Rahman, "A gas kick model that uses the thermodynamic approach to account for gas solubility in synthetic-based mud," in *SPE/IADC Middle East drilling Technology conference and exhibition*, p. D031S016R001, SPE, 2021.

[26] T. Shuren and S. Gaodong, "Application of impermeable cement cement additive in high pressure and easy lost circulation wells and its operation technology," in *International Meeting on Petroleum Engineering*, SPE, 11 1988.

[27] L. Hollman, I. Haq, C. Christenson, T. P. da Silva, M. I. B. Fayed, N. Thorn, and W. Geldof, "Developing a mpd operation matrix – case history," *SPE/IADC Drilling Conference and Exhibition*, 3 2015.

[28] A. K. Gupta, V. Sharma, A. Parasher, D. Thummar, R. S. Satyarthi, E. Rao, and S. Tiwari, "Best out of waste - waste water management for sustenance of well intervention activities," in *SPE Oil and Gas India Conference and Exhibition*, SPE, 4 2017.

[29] W. Rehm, "Abnormal pressure control maximum casing pressure from gas kicks," in *Drilling and Rock Mechanics Conference*, SPE, 1 1967.

[30] N. Al-araimi and M. Mahajan, "Successful revival of long time closed-in gas wells by right matrix stimulation treatments," in *SPE Annual Technical Conference and Exhibition*, SPE, 10 2005.

[31] B. Gedge, H. K. D. Singh, E. B. Refugio, B. T. Quoc, and N. V. Bot, "Managed pressure drilling - a solution for drilling the challenging and un-drillable wells in vietnam and south east asia," in *SPE Asia Pacific Oil and Gas Conference and Exhibition*, SPE, 10 2013.

[32] C. Leach, "Gas migration modeling improves volumetric method of well control," *Oil & Gas Journal*, 12 1994.

[33] C. S. Avelar and P. Ribeiro, "Modelagem do controle de poços por diferenças finitas," 8 2008.

[34] C. Zurdo, C. Georges, and M. Martin, "Mud and cement for horizontal wells," *SPE Annual Technical Conference and Exhibition*, 10 1986.

[35] N. Nwaka, J. Liu, M. Kunju, and Y. Chen, "Hydrodynamic modeling of gas influx migration in slim hole annuli," *Experimental and Computational Multiphase Flow*, vol. 2, pp. 142–150, 11 2019.

[36] A. Omosebi, S. O. Osisanya, G. Chukwu, and F. Egbon, “Annular pressure prediction during well control,” in *Nigeria Annual International Conference and Exhibition*, SPE, 8 2012.

[37] D. Strickland and M. Smith, “Concentric workovers successful in a well recovery operation,” 6 1997.

[38] L. W. Ledgerwood, R. W. Spencer, O. Matthews, B. J. A. Raj, J. Mendoza, and J. M. Hanson, “The effect of bit type on reactive torque and consequent tool-face-control anomalies,” *SPE Drilling & Completion*, vol. 31, pp. 95–105, 5 2016.

[39] G. Wang, C. Zhao, X. Liang, Y. Pan, L. Lin, L. Wang, Y. Rui, and Q. Li, “Integrating qualitative and quantitative drilling risk prediction methods for shale gas field in sichuan basin,” in *International Petroleum Technology Conference*, IPTC, 3 2019.

[40] S. Abbasi, C. Tyagi, and T. Chakrabarty, “Getting past the deepest barrier using plasma based punctures: A case study on the mature panna field, western offshore, india,” in *SPE Oil and Gas India Conference and Exhibition*, SPE, 4 2017.

[41] P. L. Halkyard, “Dynamics in cold atomic gases,” 8 2013.

[42] R. Guo, Y. Chen, R. P. Coutinho, and P. J. Waltrich, “Numerical and experimental investigations of gas kick migration during casing while drilling,” in *SPE Health, Safety, Security, Environment, & Social Responsibility Conference - North America*, SPE, 4 2017.

[43] H. Lima and H. C. Juvkam-Wold, “Computational hydraulic analysis of a deepwater well drilled with synthetic-based mud in a riserless drilling configuration,” *SPE Annual Technical Conference and Exhibition*, 9 1998.

[44] C. Tzotzi, T. Parenteau, D. Kaye, D. J. Turner, R. Bass, J. E. P. Morgan, E. Zakarian, J. Rolland, and M.-K. Decrin, “Safe hydrate plug dissociation in active heating flowlines and risers - full scale test,” in *Offshore Technology Conference*, OTC, 5 2016.

[45] G. Mathur, N. Tiwari, and N. Chaturvedi, “Numerical and experimental studies of ballistic compression process in a soft recovery system,” *Journal of Fluids Engineering*, vol. 143, 12 2020.

[46] K. Bybee, “Analysis of alternative well-control methods for dual-density deepwater drilling,” *Journal of Petroleum Technology*, vol. 59, pp. 61–63, 1 2007.

[47] D. R. Steele, J. Mulders, and M. Crisp, “Sable sub basin near field exploration prospectivity,” in *Offshore Technology Conference*, OTC, 5 2011.

[48] N. V. Raguzova and V. M. Lipunov, “High-eccentric x-ray binaries : Evolution, wind rose effect, accretor-propeller luminosity gap,” *Astronomy and Astrophysics*, vol. 340, pp. 85–102, 12 1998.

[49] M. F. Jamaludeen and M. A. M. Yusof, “Multiphase drilling kick annular flow behaviour in vertical and inclined well profiles,” *Platform : A Journal of Engineering*, vol. 5, pp. 23–23, 9 2021.

[50] A. N. Baushev, “Galaxy collisions as a mechanism of formation of ultra diffuse galaxies (udg),” 8 2016.

[51] R. Szczepanski, T. Yerlett, N. Brown, and T. Hamilton, “Differences between methane and condensate kicks - a simulation study,” *SPE Drilling & Completion*, vol. 13, pp. 36–41, 3 1998.

[52] A. P. Pink, H. Kverneland, A. Bruce, and J. B. Applewhite, “Building an automated drilling system where the surface machines are controlled by downhole and surface data to optimize the well construction process,” *IADC/SPE Drilling Conference and Exhibition*, 3 2012.

[53] C. H. de Oliveira Loiola, “Simulação composicional de controle de poços,” 9 2015.

[54] D. C. Thomas, J. F. Lea, and E. Turek, “Gas solubility in oil-based drilling fluids: Effects on kick detection,” 9 1983.

[55] R. Rudolf and P. Suryanarayana, “Kicks caused by tripping-in the hole on deep, high temperature wells,” in *SPE Asia Pacific Oil and Gas Conference and Exhibition*, pp. 325–333, SPE, 4 1997.

[56] W. Liu, S. Lin, Y. Zhou, and S. Fang, “The successful application of a new-style managed pressure drilling mpd equipment and technology in well penglai 9 of sichuan & chongqing district,” in *IADC/SPE Asia Pacific Drilling Technology Conference and Exhibition*, SPE, 7 2012.

[57] S. Ray and S. D. S. Sinha, “Non-equilibrium dynamics of quantum many body systems: Application to ultracold atomic gases,” 5 2019.